



# The effect of five-membered heterocyclic bridges and ethoxyphenyl substitution on the performance of phenoxazine-based dye-sensitized solar cells



Woosung Lee<sup>a</sup>, Jun Choi<sup>a</sup>, Jin Woong Namgoong<sup>a</sup>, Se Hun Kim<sup>a</sup>, Kyung Chul Sun<sup>b</sup>,  
Sung Hoon Jeong<sup>c</sup>, Kicheon Yoo<sup>d</sup>, Min Jae Ko<sup>d</sup>, Jae Pil Kim<sup>a,\*</sup>

<sup>a</sup> Department of Materials Science and Engineering, Seoul National University, Seoul 151-744, South Korea

<sup>b</sup> Department of Fuel Cells and Hydrogen Technology, Hanyang University, Seongdong-gu, Seoul 133-791, South Korea

<sup>c</sup> Department of Organic and Nano Engineering, College of Engineering, Hanyang University, Seongdong-gu, Seoul 133-791, South Korea

<sup>d</sup> Photo-Electronic Hybrids Research Center, National Agenda Research Division, Korea Institute of Science and Technology (KIST), Seoul 136-791, South Korea

## ARTICLE INFO

### Article history:

Received 7 October 2013

Accepted 20 December 2013

Available online 31 December 2013

### Keywords:

Dye-sensitized solar cells

Phenoxazine dyes

Five-membered heterocyclic bridges

Ethoxyphenyl substitution

Dihedral angle

Dye adsorption

## ABSTRACT

Phenoxazine derivatives with heterocyclic bridge units and an additional donor were synthesized and applied to dye-sensitized solar cells. To study the effects of these substituents on the DSSC performance, the photophysical, electrochemical, and photovoltaic properties of the dyes were investigated. The introduced heterocyclic bridge units furan and thiophene improved the short-circuit current due to the red-shifted absorption spectra of the dyes. The ethoxyphenyl ring introduced to the phenoxazine moiety as an additional donor broadened the spectrum of the dye, while the reduced adsorption of the dye caused by its non-planar structure limited the enhancement of the short-circuit current. Among the synthesized dyes, the one with furan as a bridge unit showed the best overall conversion efficiency of 5.26%.

© 2014 Elsevier Ltd. All rights reserved.

## 1. Introduction

Dye-sensitized solar cells (DSSCs) have attracted considerable attention as promising solar devices since Grätzel et al. reported Ru-based photosensitizers in 1991 [1]. The Ru complex dyes typical used as sensitizers in DSSCs have shown high electronic conversion efficiencies of over 11% with good stability [2]. However, high production cost and difficulties in purification have limited their development for large-scale applications. Recently, more attention has been paid to sensitizers without Ru (metal-free organic dyes and organometallic dyes) due to their lower cost, easier modification and purification, high molar extinction coefficient, and environmental friendliness. As such, sensitizers without Ru such as triphenylamine [3], indoline [4], cyanine [5], coumarin [6], perylene [7], porphyrin [8], phthalocyanine [9], and phenothiazine [10] have been extensively studied. Among these, porphyrin derivatives have shown high electronic conversion efficiency (12.3%) [7].

For efficient DSSCs, organic dyes should have broad and red-shifted absorptions in the visible region. Accordingly, most organic dyes have the structure of donor–conjugated bridges–acceptor (D– $\pi$ –A) to obtain a broad and red-shifted absorption spectrum. Among the various conjugated bridges, furan and thiophene have displayed the most remarkable results, showing wide and red-shifted absorption spectra, as well as high molar extinction coefficients [11]. In addition, to achieve enhanced photovoltaic performance, organic dyes with an additional donor (D–D–A or D–D– $\pi$ –A) have been suggested [12]. The introduction of an additional donor group could increase the electron-donating capability, which would improve electron injection and charge separation. Phenoxazine (POZ) includes electron-rich oxygen and nitrogen atoms in a heterocyclic ring, which displays high electron-donating ability [13]. It also shows sufficient electrochemical properties, which implies that POZ could be a promising sensitizer in DSSCs [14]. However, despite these advantages, POZ-based sensitizers have not been reported extensively.

In this research, to study effects of conjugated bridges with a POZ moiety on photovoltaic performance, five-membered heterocyclic rings were introduced as a conjugated bridge unit to POZ

\* Corresponding author. Tel.: +82 2 880 7187; fax: +82 2 880 7238.  
E-mail address: [jaepil@snu.ac.kr](mailto:jaepil@snu.ac.kr) (J.P. Kim).

molecules. The addition of these bridge units could extend the conjugation of the dye molecule, which red-shifted the absorption spectrum and increased the molar absorptivity of the dyes. Furthermore, to improve the donating power and molar extinction coefficient, an ethoxy phenyl ring was substituted in the 7 position of the POZ-furan dye as an additional donor.

Based on these strategies, three organic dyes (**WS1**, **WS2** and **WS3**) were designed and synthesized. The photophysical and electrochemical properties of the synthesized dyes were investigated in detail and density functional theory (DFT) calculations were also performed. Photovoltaic cells were assembled with the synthesized dyes and their photovoltaic properties were analyzed. In addition, electrochemical impedance spectroscopy (EIS) was used to study the interfacial charge transport process in the photovoltaic cells.

## 2. Experimental

### 2.1. Materials and reagents

Phenoxazine, N-bromosuccinimide and 4-ethoxyphenylboronic acid were purchased from TCI and used as received without further purification. 1-bromobutane, 5-formyl-2-furan-boronic acid, 5-formyl-2-thiophene-boronic acid, tetrakis(triphenylphosphine) palladium(0), phosphorus oxychloride, 4-ethoxyphenylboronic acid, cyanoacetic acid and piperidine were purchased from Sigma–Aldrich and used as received without further purification. All solvents (chloroform, tetrahydrofuran, dimethylformamide, dimethyl sulfoxide, dichloromethane, 1, 2-dichloroethane and acetonitrile) were obtained from Sigma–Aldrich and used as received. Other chemicals were reagent grade and used without further purification.

### 2.2. Analytical instruments and measurements

<sup>1</sup>H NMR and <sup>13</sup>C NMR spectra were recorded on a Bruker Avance 300, 500 and 600 MHz using DMSO with the chemical shift against TMS (Seoul National University National Center for Inter-University Research Facilities). Mass data were measured using a JEOL JMS 600 W mass spectrometer (Seoul National University National Center for Inter-University Research Facilities). UV–vis spectra were measured with a Hewlett–Packard 8425A spectrophotometer. Cyclic voltammetry spectra were obtained using a three-electrode cell with a 273 A potentiostat (Princeton applied research, Inc.). Measurements were performed using Ag wire (Ag/Ag<sup>+</sup>), glassy carbon and platinum wire as the reference, working and counter electrodes, respectively, in CH<sub>2</sub>Cl<sub>2</sub> solution containing 0.1 M tetrabutylammonium tetrafluoroborate (TBATFB) as the supporting electrolyte. A standard ferrocene/ferrocenium (Fc/Fc<sup>+</sup>) redox couple was employed to calibrate the oxidation peak. Photocurrent–voltage measurements were performed using a Keithley model 2400 source measure unit. A 1000 W Xe lamp (Spectra-physics) served as a light source, and it was adjusted using an NREL-calibrated silicon solar cell equipped with a KG-5 filter to approximate AM 1.5G sunlight intensity. The incident photon-to-current conversion efficiency (IPCE) was measured as a function of the wavelength from 300 nm to 800 nm using a specially designed IPCE system for dye-sensitized solar cells (PV measurements, Inc.). A 75 W Xe lamp was employed as a light source to generate a monochromatic beam. The electrical impedance spectra (EIS) of the DSSCs under dark with 0.60 V forward bias were measured with an impedance analyzer (Compactstat, IVIUM Tech) at frequencies of 10<sup>-1</sup>–10<sup>6</sup> Hz. The magnitude of the alternative signal was 10 mV. The impedance parameters were determined by fitting the impedance spectra using Z-view software.

### 2.3. Fabrication of dye-sensitized solar cells and measurements

A Photoanode paste was prepared for a screen-printing process. The final composition of the paste comprised TiO<sub>2</sub> nanopowder (1 g), ethyl cellulose (0.5 g), terpineol (3.3 mL), and acetic acid (0.16 mL). After that, pre-washed FTO glass was coated by a doctor blade process and then heated at 70 °C for 30 min for drying. After the printing, the TiO<sub>2</sub> films were heated in four steps of 325 °C, 375 °C, 450 °C, and 500 °C for 5, 5, 15, and 15 min, respectively, using a high-temperature furnace (Lab house Co.). For the post-treatment, the coated and sintered TiO<sub>2</sub> films were immersed in TiCl<sub>4</sub> solution (40 mM in water) for 30 min at 70 °C. After washing, the films were annealed at 500 °C for 30 min. Counter electrodes were prepared by spin coating method using 5 mM H<sub>2</sub>PtCl<sub>6</sub> solution (in ethanol) on one-holed FTO glass and heated at 400 °C for 20 min. After cooling at 60 °C, the TiO<sub>2</sub> electrodes were immersed in EtOH/CH<sub>2</sub>Cl<sub>2</sub> solution containing the dyes at 0.5 mM for 48 h at ambient temperature. After dye absorption, the photoanodes were washed using anhydrous ethanol and dried under nitrogen flow. The dye-covered photoelectrode and Pt-electrode were assembled using ionomer surlyn with a hot-press at 80 °C. After assembling, the electrolyte solution (composed of 0.6 M BMII, 0.05 M I<sub>2</sub>, 0.1 M LiI, and 0.5 M TBP in acetonitrile solvent) was injected into the one-holed FTO glass using a capillarity vacuum technique, and the hole was sealed with a cover-glass using the same surlyn. A black mask aperture was placed on the front electrode for better analysis of the photovoltaic characteristics. The active area of the dye-coated TiO<sub>2</sub> film was ca. 0.24 cm<sup>2</sup>, which was measured by analyzing the images from a CCD camera (moticam 1000). The TiO<sub>2</sub> film thickness was measured by an  $\alpha$ -step surface profiler (KLA Tencor).

Photocurrent–voltage (*I*–*V*) measurements were performed using a Keithley model 2400 source measure unit. A class-A solar simulator (Newport) equipped with a 150 W Xe lamp was used as the light source. The light intensity was adjusted with an NREL-calibrated Si solar cell with a KG-5 filter for approximating the light intensity of 1 sun. Photocurrent–voltage measurements of the dye-sensitized solar cells were performed with an aperture mask by following a reported method. Incident photon-to-current conversion efficiency (IPCE) was measured as a function of wavelength from 300 to 1000 nm using a specially designed IPCE system for dye-sensitized solar cells (PV measurements, Inc.). A 75 W xenon lamp was used as the light source for generating monochromatic beams. Calibration was performed using a silicon photodiode, which was calibrated based on the NIST-calibrated photodiode G425 standard. The IPCE values were measured under halogen bias light at a low chopping speed of 10 Hz. All calculations were carried out using Gaussan 09 software. Optimized geometries, energy levels, and frontier molecular orbitals of the dyes' HOMOs and LUMOs were calculated at the B3LYP/6-31G (d,p) level.

### 2.4. Synthesis of dyes

#### 2.4.1. 10-Butyl-10H-phenoxazine (**1**)

Sodium hydroxide (7.36 g, 0.184 mol) and 1-bromobutane (6.62 g, 0.048 mol) were slowly added to a phenoxazine (4.0 g, 0.022 mol) solution in dry DMSO (50 mL) at room temperature and stirred for 24 h. Then, the reaction mixture was poured into water and extracted with ethyl acetate. The organic phase was separated and dried over anhydrous MgSO<sub>4</sub>. After removing the solvent, the residue was purified by column chromatography using ethyl acetate–hexane (1:10; v/v) as the eluent to give **1**, colorless viscous liquid (4.78 g, 91%).

<sup>1</sup>H NMR (500 MHz, d<sub>6</sub>-DMSO):  $\delta$  = 6.81 (d, *J* = 8.7 Hz, 2H), 6.63–6.67 (m, 4H), 3.53 (t, *J* = 7.7 Hz, 2H), 1.50–1.54 (m, 2H), 1.38–1.43 (m, 2H), 0.94 ppm (t, *J* = 7.3 Hz, 3H).

#### 2.4.2. 10-Butyl-10H-phenoxazine-3-carbaldehyde (**2**)

POCl<sub>3</sub> (0.55 mL, 0.006 mol) was added dropwise to a solution of **1** (1.29 g, 0.005 mol) and dry DMF (5 mL) in dry 1,2-dichloroethane (10.7 mL) in an ice water bath with temperature below 15 °C. The reaction was heated to room temperature and refluxed at 90 °C for 48 h. The mixture was quenched with dilute NaOH (aq) and extracted with water and dichloromethane (DCM). The organic phase was dried with anhydrous MgSO<sub>4</sub>, and then the solvent was removed in vacuo. The residue was purified by column chromatography using ethyl acetate–hexane (1:6; v/v) to give **3**, yellow oil (0.957 g, 71.6%).

<sup>1</sup>H NMR (500 MHz, d<sub>6</sub>-DMSO): δ = 9.64 (s, 1H), 7.41 (dd, *J* = 8.3, 1.8 Hz, 1H), 7.00 (s, 1H), 6.68–6.87 (m, 5H), 3.62 (t, *J* = 7.9 Hz, 2H), 1.52–1.56 (m, 2H), 1.40–1.45 (m, 2H), 0.95 ppm (t, *J* = 7.3 Hz, 3H).

#### 2.4.3. 3-Bromo-10-butyl-10H-phenoxazine (**3a**)

**1** (1.488 g, 0.0062 mol) and N-bromosuccinimide (1.106 g, 0.0062 mol) were dissolved in chloroform (30 mL), and the reaction was stirred for 1 h at ambient temperature. The reaction was quenched with water and extracted with water and DCM. The organic phase was collected and the solvent was removed by rotary evaporation. The residue was purified by column chromatography using hexane to give **3a**, white solid (1.48 g, 75%).

<sup>1</sup>H NMR (500 MHz, d<sub>6</sub>-DMSO): δ = 7.0–6.96 (m, 1H), 6.86–6.80 (m, 2H), 6.69–6.59 (m, 4H), 3.52–3.47 (m, 2H), 1.53–1.46 (m, 2H), 1.44–1.35 (m, 2H), 0.90–0.91 ppm (m, 3H).

#### 2.4.4. 3,7-Dibromo-10-butyl-10H-phenoxazine (**3b**)

**3b** as a white solid (1.72 g, 70%) was synthesized according to the procedure described for the synthesis of **3a**. N-bromosuccinimide (2.21 g, 0.0124 mol) was added to a solution of **1** (1.49 g, 0.0062 mol) in chloroform (30 mL) at ambient temperature. Eluent: hexane.

<sup>1</sup>H NMR (500 MHz, d<sub>6</sub>-DMSO): δ = 7.0 (d, *J* = 8.6 Hz, 2H), 6.83 (s, 2H), 6.54 (d, *J* = 8.7 Hz, 1H), 3.50 (t, *J* = 7.5 Hz, 2H), 1.50–1.45 (m, 2H), 1.40–1.36 (m, 2H), 0.92 ppm (t, *J* = 7.3 Hz, 3H).

#### 2.4.5. 5-(10-Butyl-10H-phenoxazin-3-yl)furan-2-carbaldehyde (**4a**)

Under nitrogen atmosphere, a mixture of **3a** (2.21 g, 0.0069 mol), 5-formyl-2-furan-boronic acid (1.12 g, 0.0080 mol), 2 M aqueous of K<sub>2</sub>CO<sub>3</sub> (8.66 mL), Pd(PPh<sub>3</sub>)<sub>4</sub> (0.4 g, 0.00035 mol) in dry THF (100 mL) was stirred for 1/2 h and refluxed at 80 °C overnight. The reaction was extracted with DCM, water and brine. The organic phase was dried with anhydrous MgSO<sub>4</sub>, and then the solvent was removed in vacuo. The residue was purified by column chromatography using DCM-hexane (5:1; v/v) to give **4a**, orange oil (1.13 g, 49%).

<sup>1</sup>H NMR (500 MHz, d<sub>6</sub>-DMSO): δ = 9.53 (s, 1H), 7.60 (s, 1H), 7.33 (d, *J* = 8.4 Hz, 1H), 7.12 (s, 1H), 7.11 (s, 1H), 6.86 (t, *J* = 7.9 Hz, 1H), 6.78 (d, *J* = 8.5 Hz, 1H), 6.74–6.66 (m, 3H), 3.59 (t, *J* = 7.6 Hz, 2H), 1.57–1.52 (m, 2H), 1.45–1.40 (m, 2H), 0.95 ppm (t, *J* = 7.3 Hz, 3H).

#### 2.4.6. 5-(10-Butyl-10H-phenoxazin-3-yl)thiophene-2-carbaldehyde (**4b**)

**4b** as an orange oil (1.53 g, 42%) was synthesized according to the procedure described for the synthesis of **4a**. 5-formyl-2-thiophene-boronic acid (1.95 g, 0.0124 mol) was added under nitrogen atmosphere to a solution of **3a** (3.32 g, 0.0104 mol), 2 M aqueous K<sub>2</sub>CO<sub>3</sub> (13 mL), Pd(PPh<sub>3</sub>)<sub>4</sub> (0.61 g, 0.00053 mol) in dry THF (100 mL). Eluent: DCM-hexane (5:1; v/v).

<sup>1</sup>H NMR (300 MHz, d<sub>6</sub>-DMSO): δ = 9.84 (s, 1H), 7.96 (s, 1H), 7.59 (s, 1H), 7.26 (d, *J* = 8.3 Hz, 1H), 7.09 (s, 1H), 6.88–6.84 (m, 1H), 6.75–6.66 (m, 4H), 3.59 (t, *J* = 7.9 Hz, 2H), 1.55–1.48 (m, 2H), 1.46–1.38 (m, 2H), 0.95 ppm (t, *J* = 7.2 Hz, 3H).

#### 2.4.7. 3-(5-Formyl-2-furan)-7-bromo-10-butyl-10H-phenoxazine (**4c**)

**4c** as an orange oil (1.03 g, 41%) was synthesized according to the procedure described for the synthesis of **4a**. 5-formyl-2-furan-boronic acid (1.02 g, 0.0072 mol) was added under nitrogen atmosphere to a solution of **3b** (2.41 g, 0.0061 mol), 2 M aqueous K<sub>2</sub>CO<sub>3</sub> (15.25 mL), Pd(PPh<sub>3</sub>)<sub>4</sub> (0.71 g, 0.00061 mol) in dry THF (100 mL). Eluent: DCM-hexane (5:1; v/v).

<sup>1</sup>H NMR (500 MHz, d<sub>6</sub>-DMSO): δ = 9.53 (s, 1H), 7.60 (s, 1H), 7.35 (d, *J* = 8.4 Hz, 1H), 7.13 (m, 2H), 7.02 (d, *J* = 8.4 Hz, 1H), 6.85 (s, 1H), 6.82 (d, *J* = 8.6 Hz, 1H), 6.68 (d, *J* = 8.7 Hz, 1H), 3.58 (t, *J* = 7.5 Hz, 2H), 1.54–1.50 (m, 2H), 1.43–1.39 (m, 2H), 0.94 ppm (t, *J* = 7.3 Hz, 3H).

#### 2.4.8. 5-(3-(4-Ethoxyphenyl)-10-butyl-10H-phenothiazin-7-yl)furan-2-carbaldehyde (**5a**)

A mixture of **4c** (0.5 g, 0.0012 mol), 2 M aqueous K<sub>2</sub>CO<sub>3</sub> (6 mL), Pd(PPh<sub>3</sub>)<sub>4</sub> (0.07 g, 0.00006 mol) in dry THF (15 mL) was refluxed for 1/2 h. 4-ethoxyphenylboronic acid (0.28 g, 0.0017 mol) dissolved in dry THF (5 mL) was added to the reaction mixture and refluxed for 15 h. The mixture was quenched with water and extracted with DCM. The organic phase was dried with anhydrous MgSO<sub>4</sub>, and then the solvent was removed in vacuo. The residue was purified by column chromatography using DCM-ethyl acetate (10:1; v/v) to give **5a**, orange oil (0.29 g, 53%).

<sup>1</sup>H NMR (500 MHz, d<sub>6</sub>-DMSO): δ = 9.52 (s, 1H), 7.57 (s, 1H), 7.49 (d, *J* = 8.7 Hz, 2H), 7.34 (d, *J* = 8.4 Hz, 2H), 7.13–7.07 (m, 3H), 6.94 (d, *J* = 8.7 Hz, 2H), 6.91 (s, 1H), 6.77 (t, *J* = 8.7 Hz, 2H), 4.06–4.00 (m, 2H), 3.62 (t, *J* = 7.5 Hz, 2H), 1.58–1.56 (m, 2H), 1.45–1.43 (m, 2H), 1.34 (t, *J* = 7 Hz, 3H), 0.97 ppm (t, *J* = 7.3 Hz, 3H).

#### 2.4.9. (E)-(10-Butyl-10H-phenoxazin-3-yl)-2-cyanoacrylic acid (**POX**)

**3** (0.23 g, 0.00086 mol), cyanoacetic acid (0.22 g, 0.0026 mol) and piperidine (0.18 mL, 0.00347 mol) were added to anhydrous CH<sub>3</sub>CN (100 mL). After the mixture was refluxed for 8 h, the solution was extracted with DCM and 0.1 M HCl aqueous solution. The organic phase was dried over anhydrous MgSO<sub>4</sub>, and the solvent was removed in vacuo. The crude product was purified by column chromatography using DCM-methanol (5:1; v/v) to give **POX**, red solid (0.22 g, 75%).

<sup>1</sup>H NMR (600 MHz, d<sub>6</sub>-DMSO): δ = 7.97 (s, 1H), 7.48 (d, *J* = 8.5 Hz, 1H), 7.36 (s, 1H), 6.85 (t, *J* = 7.6 Hz, 1H), 6.69–6.78 (m, 4H), 3.59 (t, *J* = 7.6 Hz, 2H), 1.50–1.55 (m, 2H), 1.37–1.43 (m, 2H), 0.93 ppm (t, *J* = 7.3 Hz, 3H).

<sup>13</sup>C NMR (150 MHz, d<sub>6</sub>-DMSO): δ = 164.1, 152.2, 143.8, 143.6, 137.8, 130.9, 130.6, 124.3, 123.7, 122.6, 117.2, 115.3, 114.5, 112.9, 111.7, 98.0, 42.9, 26.7, 19.2, 13.7 ppm; *m/z* (FAB) 334.1316 ((M<sup>+</sup>), C<sub>20</sub>H<sub>18</sub>N<sub>2</sub>O<sub>3</sub> requires 334.1317).

#### 2.4.10. (E)-3-(5-(10-Butyl-10H-phenoxazin-3-yl)furan-2-yl)-2-cyanoacrylic acid (**WS1**)

**WS1** (0.13 g, 54%) was synthesized according to the procedure described for the synthesis of **POX**. **4a** as a dark red solid (0.2 g, 0.0006 mol), cyanoacetic acid (0.15 g, 0.0018 mol), and piperidine (0.24 mL, 0.0024 mol) were added to anhydrous CH<sub>3</sub>CN (50 mL). Eluent: DCM-methanol (9:1; v/v).

<sup>1</sup>H NMR (500 MHz, d<sub>6</sub>-DMSO): δ = 7.97 (s, 1H), 7.48 (s, 1H), 7.41 (d, *J* = 8 Hz, 1H), 7.19–7.17 (m, 2H), 6.87–6.84 (m, 1H), 6.81 (d, *J* = 9 Hz, 1H), 6.74–6.72 (m, 1H), 6.70–6.68 (m, 2H), 3.60 (t, *J* = 7.5 Hz, 2H), 1.58–1.52 (m, 2H), 1.46–1.39 (m, 2H), 0.95 ppm (t, *J* = 7.5 Hz, 3H).

<sup>13</sup>C NMR (125 MHz, d<sub>6</sub>-DMSO): δ = 163.5, 158.0, 146.4, 143.7, 143.2, 136.4, 133.9, 131.1, 126.2, 123.7, 121.1, 121.0, 120.4, 116.4, 114.6, 111.9, 111.8, 110.6, 108.0, 42.6, 26.1, 18.7, 13.2 ppm; *m/z* (FAB) 400.1422 ((M<sup>+</sup>), C<sub>24</sub>H<sub>20</sub>N<sub>2</sub>O<sub>4</sub> requires 400.1423).

#### 2.4.11. (E)-3-(5-(10-Butyl-10H-phenoxazin-3-yl)thiophene-2-yl)-2-cyanoacrylic acid (**WS2**)

**WS2** (0.43 g, 79%) as a dark red solid was synthesized according to the procedure described for the synthesis of **POX**. **4b** (0.46 g, 0.0013 mol), cyanoacetic acid (0.33 g, 0.0039 mol), and piperidine (0.51 mL, 0.0052 mol) were added to anhydrous  $\text{CH}_3\text{CN}$  (100 mL). Eluent: DCM-methanol (10:1; v/v).

$^1\text{H}$  NMR (500 MHz,  $d_6$ -DMSO):  $\delta$  = 8.43 (s, 1H), 7.96 (s, 1H), 7.63 (s, 1H), 7.25 (d,  $J$  = 8.5 Hz, 1H), 7.08 (s, 1H), 6.87 (t,  $J$  = 7.5 Hz, 1H), 6.77–6.69 (m, 4H), 3.61 (t,  $J$  = 6.5 Hz, 2H), 1.59–1.53 (m, 2H), 1.47–1.40 (m, 2H), 0.96 ppm (t,  $J$  = 7 Hz, 3H).

$^{13}\text{C}$  NMR (75 MHz,  $d_6$ -DMSO):  $\delta$  = 163.2, 151.9, 145.8, 143.8, 143.1, 141.0, 133.8, 132.6, 131.3, 124.2, 123.8, 123.2, 122.1, 121.0, 116.2, 114.6, 111.9, 111.6, 66.4, 26.0, 18.8, 13.2 ppm;  $m/z$  (FAB) 417.1281 (( $\text{M} + \text{H}^+$ ),  $\text{C}_{24}\text{H}_{21}\text{N}_2\text{O}_3$  S requires 417.1273).

#### 2.4.12. (E)-3-(5-(4-Methoxyphenyl)-10-butyl-10H-phenoxazin-7-yl)furan-2-yl)-2-cyanoacrylic acid (**WS3**)

**WS3** (0.25 g, 72%) as a dark purple solid was synthesized according to the procedure described for the synthesis of **POX**. **5a** (0.3 g, 0.00066 mol), cyanoacetic acid (0.17 g, 0.002 mol) and piperidine (0.26 mL, 0.0026 mol) were added to anhydrous  $\text{CH}_3\text{CN}$  (100 mL). Eluent: DCM-methanol (5:1; v/v).

$^1\text{H}$  NMR (500 MHz,  $d_6$ -DMSO):  $\delta$  = 7.98 (s, 1H), 7.54 (d,  $J$  = 8.5 Hz, 2H), 7.49 (s, 1H), 7.44 (d,  $J$  = 8.5, 1H), 7.22–7.20 (m, 2H), 7.13 (d,  $J$  = 8 Hz, 1H), 6.95 (m, 3H), 6.86 (d,  $J$  = 8.5 Hz, 1H), 6.80 (d,  $J$  = 8.5 Hz, 1H), 4.06–4.05 (m, 2H), 3.65 (t,  $J$  = 7 Hz, 2H), 1.59–1.57 (m, 2H), 1.48–1.43 (m, 2H), 1.34 (d,  $J$  = 7 Hz, 3H), 0.97 ppm (t,  $J$  = 7 Hz, 3H).

$^{13}\text{C}$  NMR (75 MHz,  $d_6$ -DMSO):  $\delta$  = 163.5, 158.1, 157.3, 146.4, 143.6, 143.5, 136.5, 133.7, 132.8, 130.5, 129.8, 126.3, 121.3, 121.0, 120.4, 120.4, 116.4, 114.2, 112.3, 112.1, 111.9, 110.6, 108.2, 62.5, 42.2, 26.2, 18.8, 14.1, 13.3 ppm;  $m/z$  (FAB) 500.2002 (( $\text{M}^+$ ),  $\text{C}_{32}\text{H}_{28}\text{N}_2\text{O}_5$  requires 500.1998).

### 3. Results and discussion

#### 3.1. Synthesis

The synthetic routes of POZ dyes are shown in Scheme 1 and the synthesized dyes and reference dyes (**POX**) were shown in Fig. 1. The POZ syntheses first involved an alkylation reaction on POZ nitrogen atom and a butyl chain was introduced to the POZ moiety

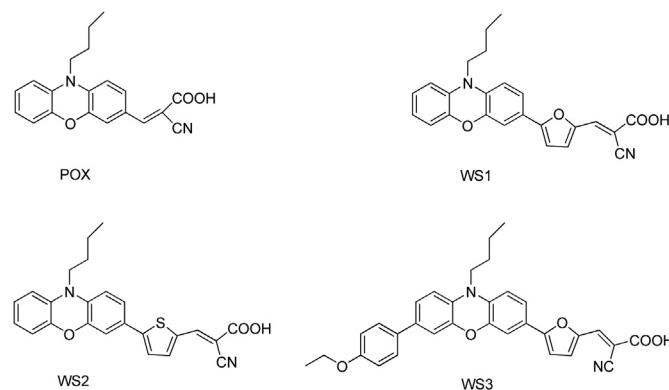
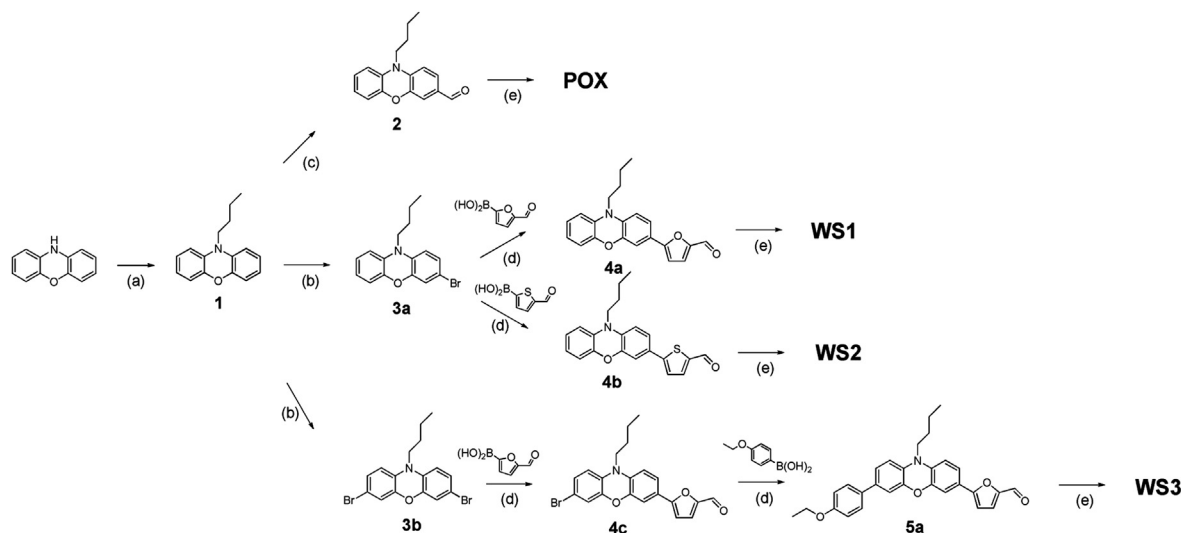


Fig. 1. Structure of **POX**, **WS1**, **WS2**, and **WS3**.

to give intermediate **1**. The bromination of **1** was performed by varying the amount of N-bromosuccinimide (NBS) to provide mono-brominated **3a** and dibrominated **3b**, respectively. The Suzuki coupling reactions of **3a** were carried out with 5-formyl-2-furanboronic acid or 5-formyl-2-thiopheneboronic acid, which produced **4a** and **4b**, respectively. The Suzuki coupling reaction of **3b** to give **4c** followed the procedure performed with **3a**, and subsequently, an additional Suzuki coupling reaction of **4c** with 4-ethoxyphenylboronic acid gave **5a**. The final compounds (**WS1**, **WS2**, and **WS3**) were obtained by the Knoevenagel reactions of the corresponding aldehydes (**4a**, **4b**, and **5a**) with cyanoacetic acid in the presence of piperidine [15]. The reference dye (**POX**) was obtained by previously reported synthetic routes. The structures of all the synthesized intermediates and dyes were identified by  $^1\text{H}$  NMR, and the final products were additionally confirmed by  $^{13}\text{C}$  NMR and HRMS.

#### 3.2. Photophysical properties

The absorption spectra of the dyes in EtOH/ $\text{CH}_2\text{Cl}_2$  solution and on the  $\text{TiO}_2$  surface are shown in Fig. 2, and the corresponding photophysical data are listed in Table 1. All the dyes exhibited two major absorption bands, which appeared at below 350 nm and 400–550 nm, respectively. The former band in the UV region is ascribed to a localized aromatic  $\pi$ – $\pi^*$  transition, and the latter



Scheme 1. Synthesis of **POX**, **WS1**, **WS2**, and **WS3**: (a) 1-iodobutane, NaOH, DMSO (b) NBS,  $\text{CHCl}_3$  (c)  $\text{POCl}_3$ , DMF,  $\text{CHCl}_3$  (d) 20 M aqueous of  $\text{K}_2\text{CO}_3$ ,  $\text{Pd}(\text{PPh}_3)_4$ , THF (e) cyanoacetic acid, piperidine, acetonitrile.

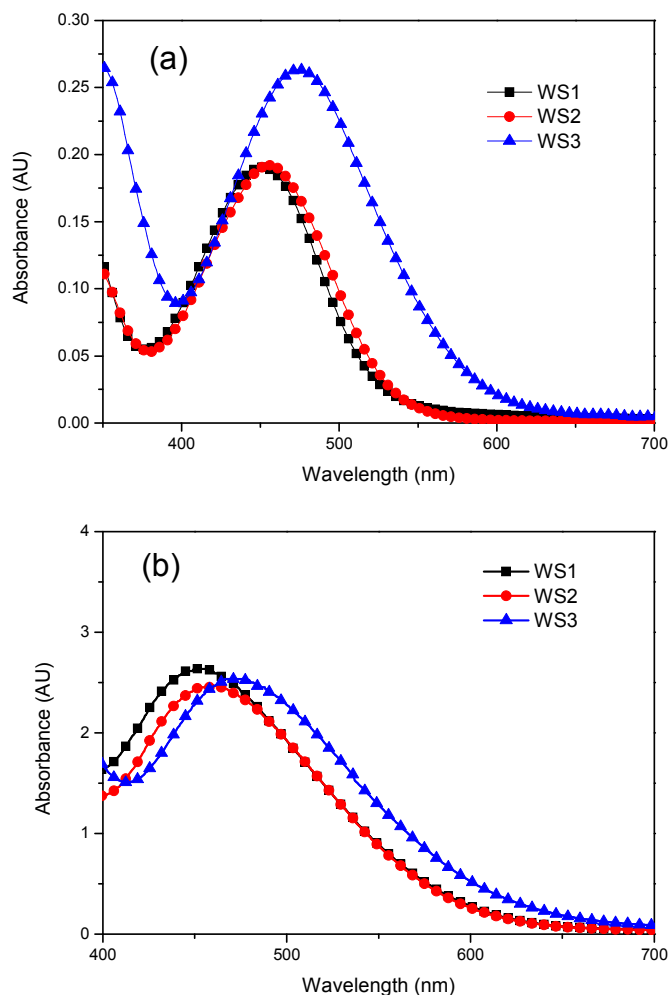


Fig. 2. Absorption spectra of **WS1**, **WS2** and **WS3** in (a) EtOH/CH<sub>2</sub>Cl<sub>2</sub> (7:2; v/v) ( $10^{-5}$  mol L<sup>-1</sup>) and (b) on TiO<sub>2</sub>.

band in the visible region is due to the intramolecular charge-transfer (ICT) transition from the donor to the acceptor. The absorption maxima ( $\lambda_{\max}$ ) of **WS1**, **WS2**, and **WS3** are 452, 455, and 475 nm, respectively. The absorption spectrum of **WS3**, which included both the additional donor and bridge moiety, was red-shifted more than 10 nm compared to those of **WS1** and **WS2**, which included the bridge unit only. This was attributed to the better delocalization of electrons over the  $\pi$ -conjugated molecules by both the electron-rich furan and the ethoxy phenyl ring. The

Table 1  
Photophysical and electrochemical properties of **WS1**, **WS2** and **WS3** dyes.

Dye	Absorption <sup>a</sup>			Oxidation potential data <sup>c</sup>		
	$\lambda_{\max}$ /nm	$\epsilon$ /M <sup>-1</sup> cm <sup>-1</sup> (at $\lambda_{\max}$ )	$\lambda_{\text{abs}}^b$ /nm (on TiO <sub>2</sub> )	$E_{\text{ox}}$ /V (vs. NHE)	$E_{0-0}^d$ /V	$E_{\text{ox}} - E_{0-0}$ V (vs. NHE)
<b>WS1</b>	452	19,063	449	0.88	2.36	-1.48
<b>WS2</b>	455	19,209	452	0.89	2.33	-1.44
<b>WS3</b>	475	26,335	466	0.81	2.13	-1.31

<sup>a</sup> Measured in  $1 \times 10^{-5}$  EtOH/CH<sub>2</sub>Cl<sub>2</sub> solutions at room temperature.

<sup>b</sup> Measured on TiO<sub>2</sub> film.

<sup>c</sup> Measured in CH<sub>2</sub>Cl<sub>2</sub> containing 0.1 M tetrabutylammonium tetrafluoroborate. (TBABF<sub>4</sub>) electrolyte (working electrode: glassy carbon; counter electrode: Pt; reference electrode: Ag/Ag<sup>+</sup>; calibrated with ferrocene/ferrocenium (Fc/Fc<sup>+</sup>) as an internal reference and converted to NHE by addition of 630 mV).

<sup>d</sup> Estimated from onset wavelength in absorption spectra.

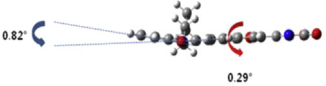
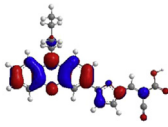
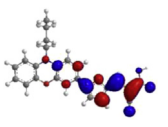
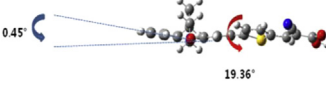
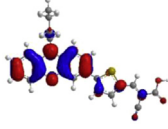
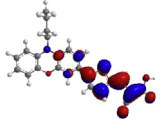
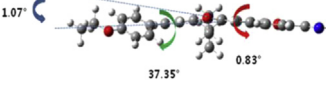
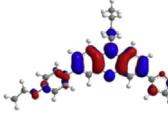
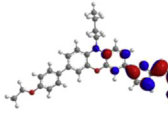
molar extinction coefficient at  $\lambda_{\max}$  of **WS1**, **WS2**, and **WS3** were 19,063, 19,209, and 26,335 M<sup>-1</sup> cm<sup>-1</sup>, respectively. These are higher than those of structurally similar phenothiazine dyes (PT 5, 17,600 M<sup>-1</sup> cm<sup>-1</sup>) as well as standard ruthenium dye (N719, 14,000 M<sup>-1</sup> cm<sup>-1</sup>), which afford the use of thinner TiO<sub>2</sub> film for efficient electron diffusion. Among these dyes, **WS3** exhibited the highest molar extinction coefficient. This result indicated that the ethoxy phenyl ring is beneficial to the conjugation and absorption properties of **WS3**, despite the large dihedral angle between the POZ core and ethoxy phenyl ring (Table 2). The red-shifts in the absorption spectra and high molar extinction coefficients of the dyes have a tendency to increase with enhancement of the electron density in the bridge unit and additional donor. Thus, their introduction to the POZ moiety is favorable for enhancing the light harvest and photocurrent generation of the dyes.

The absorption spectra of the dyes adsorbed on TiO<sub>2</sub> film are blue-shifted compared to those in solution, and there is a larger blue-shift in **WS3** (9 nm) than in **WS1** and **WS2** (3 nm). This might be due to the H-aggregation of the dyes or the deprotonation of carboxylic acid upon the adsorption onto the TiO<sub>2</sub> surface [16]. **WS3** showed almost the same absorbance on the TiO<sub>2</sub> surface compared to **WS1** and **WS2**, although it exhibited a much higher molar extinction coefficient in solution. As shown in Tables 2 and 3, this is due to the non-planar structure of **WS3** caused by the introduction of the ethoxy phenyl ring, which inhibits the adsorption of the dye on the TiO<sub>2</sub> surface. The optimized geometry of the dye in the ground state revealed that the POZ core of all the dyes had planar structures with small torsion angles (0.82–1.07°). On the other hand, there were considerable differences in the dihedral angles between the POZ core and the substituents. **WS1** had almost planar structure with a small dihedral angle (0.29°) between the core of the dye and the furan moiety, while, the planarity of **WS2** and **WS3** decreased significantly due to the large dihedral angle between the POZ core and the adjacent bridge unit or donor moiety; the dihedral angle between thiophene and the POZ core in **WS2** was 19.36°, and that between the ethoxy phenyl ring and the POZ core in **WS3** was 37.35°. **WS3** had the most twisted molecular geometry of the dyes, which led to less adsorption and decreased absorbance of the dye on the TiO<sub>2</sub> surface (Table 3).

### 3.3. Electrochemical properties

The electrochemical properties and energy levels of the prepared dyes are provided in Table 1 and Fig. 3. The oxidation potentials of the dyes were measured using cyclic voltammetry (CV), and the C–V curves of the dyes are shown in Fig. 4. The HOMO levels of the prepared dyes correspond to the first oxidation potential vs. a normal hydrogen electrode (vs. NHE) calibrated by Fc/Fc<sup>+</sup> (with 640 mV vs. NHE). All of the HOMO levels of the dyes ranged from 0.81 eV to 0.88 eV (vs. NHE) and were sufficiently positive compared to the redox potential of I<sup>-</sup>/I<sub>3</sub><sup>-</sup> (0.4 V vs. NHE), implying that the oxidized dyes can be effectively regenerated by the redox electrolyte [17]. The LUMO levels of the dyes were obtained by subtracting the zeroth–zeroth energy ( $E_{0-0}$ ) from  $E_{\text{ox}}$ , in which the zeroth–zeroth energy of the dyes is determined from the inflection point at the end of the visible absorption spectrum of the dyes. All of the LUMO levels of the dyes were more negative than the conduction band energy level ( $E_{\text{cb}}$ ) of TiO<sub>2</sub> (-0.5 vs. NHE), indicating that the excited electrons of the dyes can be efficiently injected into the conduction band of TiO<sub>2</sub>, and oxidized dyes are simultaneously formed [17]. As shown in Table 1, **WS3** had a more negative HOMO level and a more positive LUMO level than **WS1** and **WS2**. This might be attributed to the extension of conjugation induced by the additional donating group. Consequently, the gap

**Table 2**  
Optimized structures, dihedral angles and electronic distributions in HOMO and LUMO levels of the prepared dyes.

Dye	Optimized structure	HOMO	LUMO
WS1			
WS2			
WS3			

**Table 3**  
DSSC performance parameters of **POX**, **WS1**, **WS2**, and **WS3**.<sup>a</sup>

Dye <sup>b</sup>	$J_{sc}$ (mA/cm <sup>2</sup> )	$V_{oc}$ (mV)	FF (%)	$\eta$ (%)	Dye amount <sup>c</sup> (10 <sup>-7</sup> mol cm <sup>-2</sup> )
<b>POX</b>	9.88	663.5	73.22	4.80	–
<b>WS1</b>	11.72	653.0	68.76	5.26	2.05
<b>WS2</b>	11.11	628.3	70.38	4.91	1.89
<b>WS3</b>	11.35	639.9	67.09	4.87	1.34
<b>N719</b>	14.71	728.3	72.85	7.80	–

<sup>a</sup> Measured under AM 1.5 irradiation G (100 mW cm<sup>-2</sup>); 0.2 cm<sup>2</sup> working area.

<sup>b</sup> Dyes were maintained at 0.5 mM in EtOH/CH<sub>2</sub>Cl<sub>2</sub> solution, with 10 mM CDCA co-adsorbent. Electrolyte comprised 0.7 M 1-propyl-3-methyl-imidazolium iodide (PMII), 0.2 M LiI, 0.05 M I<sub>2</sub>, 0.5 M TBP in acetonitrile-valeronitrile (v/v, 85/15) for organic dyes.

<sup>c</sup> Dyes' adsorption on TiO<sub>2</sub> were measured by a colorimetric method using 0.1 M NaOH aqueous-DMF (1:1) mixed solutions to wash the dyes from 8 μm thick TiO<sub>2</sub> film.

between the HOMO and LUMO decreased, and the absorption spectra became red-shifted.

### 3.4. Photovoltaic properties

DSSCs were fabricated using the dyes as sensitizers, and their photovoltaic properties were measured under the standard AM

1.5G irradiation conditions (100 mW cm<sup>-2</sup>). The effects of the five-membered heterocyclic bridges and the ethoxyphenyl substitution on the performance of the cells were evaluated by measuring their conversion efficiency relative to the reference dye (**POX**). The IPCE spectra and photocurrent–voltage ( $J$ – $V$ ) curves are shown in Fig. 5, and the corresponding data are listed in Table 3. All the dyes showed high maximum IPCE values at 400–500 nm, which were 73.4%, 69.7%, and 73.2% for **WS1**, **WS2**, and **WS3**, respectively. These values were higher than that of standard ruthenium dye (N719, 69.6%). Therefore, all the dyes can effectively convert visible light into photocurrent in the absorption ranges. The IPCE spectra of **WS1** and **WS2** showed broadened and red-shifted ranges compared to that of **POX**, and the onsets of their IPCE spectra were extended to 750 nm. The bridge units introduced to the POZ moiety red-shifted the spectra of the dyes due to the extension of conjugation, increasing light harvest in the long wavelength region. **WS3**, which had an additional donor, showed a similar IPCE spectrum to that of **WS1**. This might be attributed to the fact that the absorption spectrum of **WS3** on TiO<sub>2</sub> was largely blue-shifted compared to that of **WS1**. In addition, it is known that a larger amount of dye adsorbed on TiO<sub>2</sub> leads to a broader IPCE spectrum [18]. Thus, the lesser amount of adsorption of **WS3** on the TiO<sub>2</sub> surface also contributed the relatively narrow IPCE spectrum of the dye. The short-circuit current ( $J_{sc}$ ) values increased in the order of

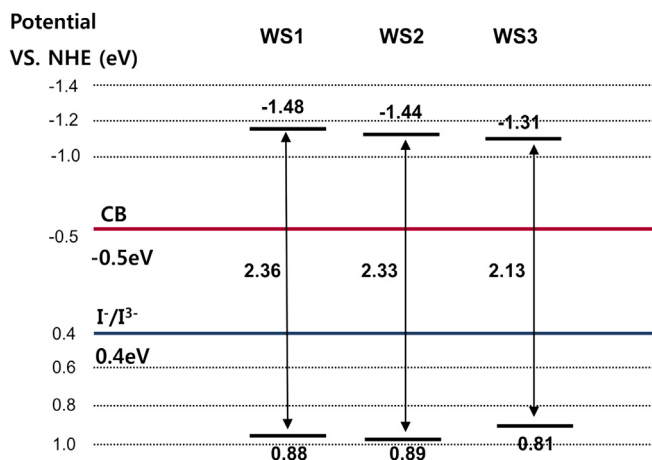


**Fig. 3.** Dyes' HOMO and LUMO energy levels.

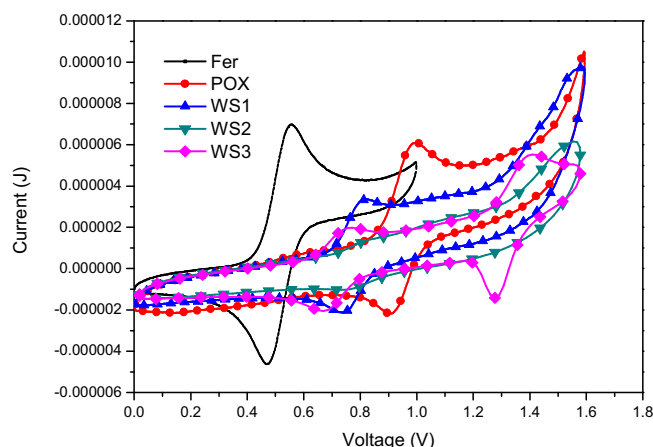


**Fig. 4.** CV curves of Fc/Fc<sup>+</sup>, **POX**, **WS1**, **WS2**, and **WS3** in CH<sub>2</sub>Cl<sub>2</sub>.

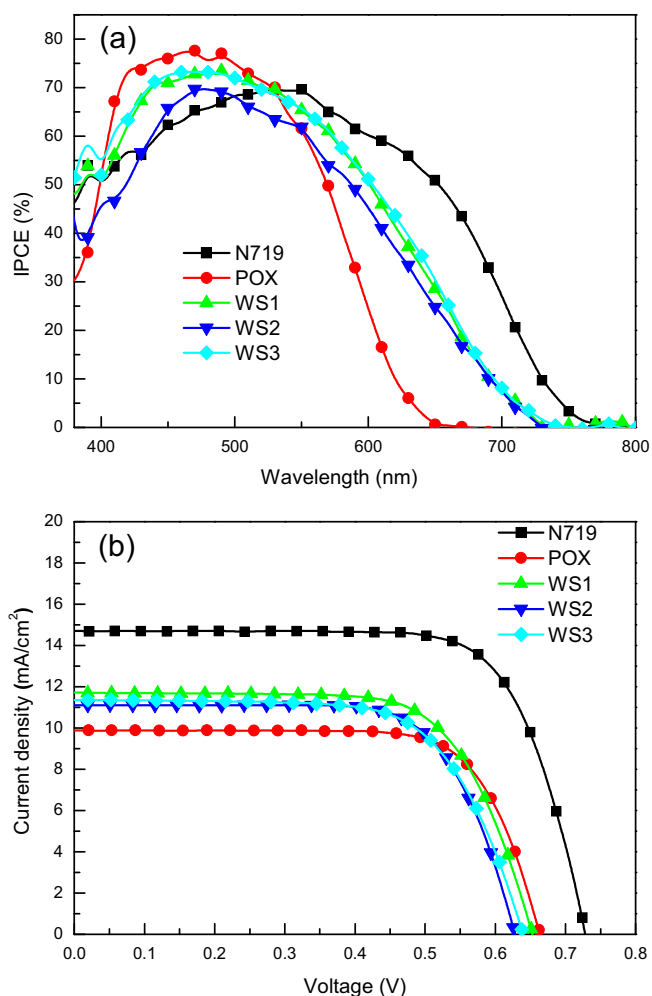


Fig. 5. (a) IPCE spectra DSSCs based on POX, WS1, WS2, WS3 and N719 and (b) the DSSCs'  $J$ - $V$  curves under AM 1.5G simulated sunlight (100  $\text{mW cm}^{-2}$ ).

POX < WS2 < WS3 < WS1, and this trend correlated with the broadness of the IPCE spectrum. Consequently, the introduced bridge units improved  $J_{sc}$  and the conversion efficiency, while the introduction of the additional donor group to the POZ moiety had little effect on  $J_{sc}$ .

The open-circuit voltage ( $V_{oc}$ ) values of the cells fabricated with the dyes increased in the order of WS2 < WS3 < WS1 < POX. The  $V_{oc}$  values of the cells based on WS1-3 are lower than that based on POX. As shown in previous studies, this might be explained by the increased interaction caused by the introduction of a heterocyclic bridge unit from  $\pi$ - $\pi$  interaction between the dye molecules and/or the interaction between the heteroatom in the bridge unit and iodine [19], [11b]. These interactions enhanced the charge recombination at the dye/dye or dye/electrolyte interface, resulting in low  $V_{oc}$  values of the cells. As shown in Fig. 6, this tendency was also shown in the dark currents of the cells made with the dyes. The dark current is defined as the relatively small electric current flowing out of a system without illumination and lower dark current indicates decreased recombination and high  $V_{oc}$ . Thus, the low dark current of the cell with POX corresponds with the highest  $V_{oc}$ , whereas the high dark current of the cell with WS2 is consistent with the lowest  $V_{oc}$ .

To explain the correlation between the  $V_{oc}$  of the cells and the dyes, electrochemical impedance spectroscopy (EIS) [20] was

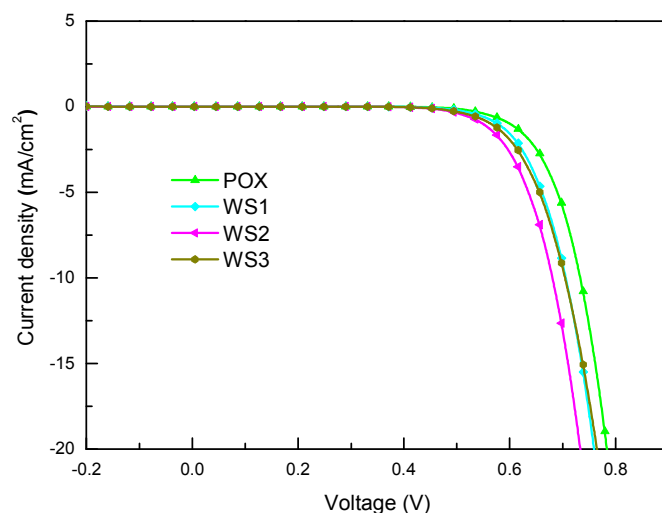


Fig. 6. DSSCs'  $J$ - $V$  curves based on POX, WS1, WS2 and WS3 in the dark.

carried out in the dark under a forward bias of  $-0.60$  V. The Nyquist plots of the DSSCs fabricated with the dyes are shown in Fig. 7. In the Nyquist plot, the major semicircle at the intermediate frequency represents the charge transfer impedance at the  $\text{TiO}_2/\text{dye}/\text{electrolyte}$  interface. The charge recombination resistance can be estimated by the radius of the major semicircle, with a larger radius of the major semicircle meaning a smaller charge recombination rate [21]. The charge recombination resistance increased in the order of WS2 < WS3 < WS1 < POX, which is in accordance with the  $V_{oc}$  values in the DSSCs made with the dyes. As the charge recombination between injected electrons and the electrolyte increased,  $V_{oc}$  increased as well. As shown in Fig. 8, this result coincides with the electron lifetime vs. dark bias voltage. The electron lifetime increased in the order of WS2 < WS3  $\approx$  WS1 < POX < N719. Longer electron lifetime indicates improved charge recombination resistance between the injected electrons and electrolyte, with a consequent increase in the  $V_{oc}$  [22]. The results suggest that the introduction of the furan bridge unit retards the charge recombination more effectively compared to the thiophene bridge unit, leading to a longer electron lifetime and a higher  $V_{oc}$ .

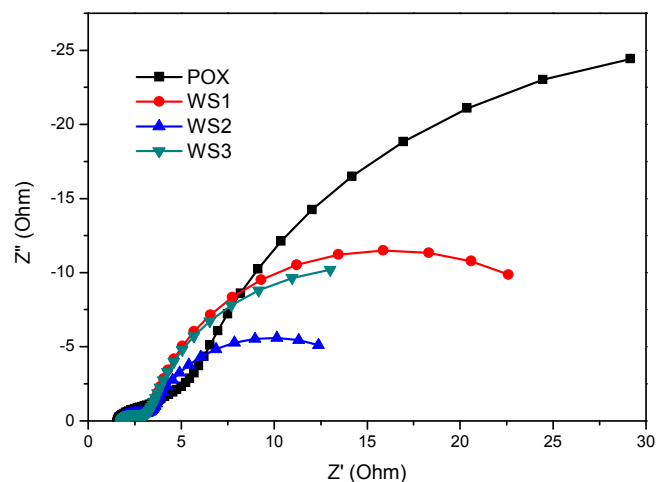


Fig. 7. Impedance spectra of DSSCs based on POX, WS1, WS2, and WS3; Nyquist plots measured at 0.60 V forward bias in the dark.

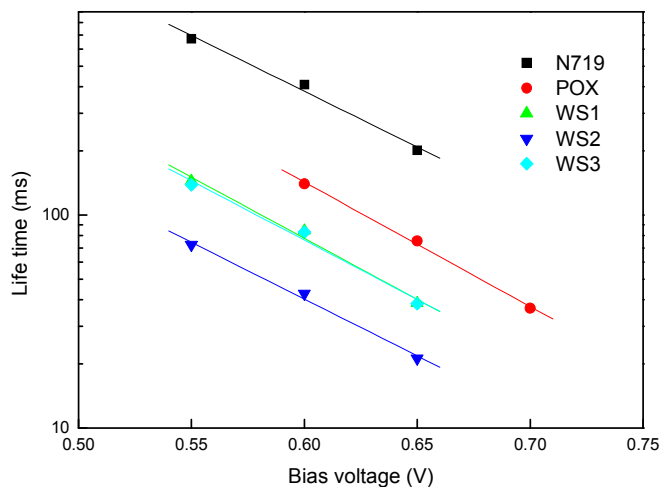


Fig. 8. Electron lifetime of N719, POX, WS1, WS2, and WS3 as a function of bias voltage.

#### 4. Conclusion

The first design and synthesis of three novel phenoxazine-based organic dyes (WS1, WS2 and WS3) has been done to study the effects of the various bridge units and an additional donor on the performance of DSSCs. The introduction of the heterocyclic bridge units (furan and thiophene) extended the conjugation and red-shifted the absorption spectra of the dyes, improving  $J_{sc}$ . Consequently, the DSSCs based on WS1 with the furan unit and WS2 with the thiophene unit showed higher overall conversion efficiencies in comparison with the reference dye (POX) without the bridge unit. The most effective bridge unit was furan, which had a higher recombination resistance and  $V_{oc}$  value. WS3 with the ethoxy phenyl ring as an additional donor showed more red-shift in the absorption, whereas the planarity of the dye was reduced by the large dihedral angle between the ethoxy phenyl ring and the POZ core. This non-planar structure of the dye led to less adsorption of the dye on the  $TiO_2$  surface, which limited the  $J_{sc}$  enhancement. The DSSC based on WS1 with the furan bridge unit exhibited the highest overall conversion efficiency of 5.26% ( $J_{sc} = 11.72 \text{ mA/cm}^2$ ,  $V_{oc} = 653 \text{ mV}$ ,  $FF = 68.76$ ).

#### Acknowledgments

This work was supported by a Grant-in-Aid for the Industrial Strategic Technology Program from the Korea Ministry of Knowledge Economy (No. 10038599).

#### References

- [1] O'Regan B, Grätzel M. A low-cost, high-efficiency solar cell based on dye-sensitized colloidal  $TiO_2$  films. *Nature* 1991;353:737–40.
- [2] (a) Grätzel M. Dye-sensitized solar cells. *J Photochem Photobiol C* 2003;4:145–53; (b) Grätzel M. Conversion of sunlight to electric power by nanocrystalline dye-sensitized solar cells. *J Photochem Photobiol* 2004;164(3):3–14; (c) Park N-G, Kim K. Transparent solar cells based on dye-sensitized nanocrystalline semiconductors. *Phys Status Solidi (a)* 2008;205(8):1895–904.
- [3] (a) Zeng WD, Cao Y, Bai Y, Wang Y, Shi Y, Zhang M, et al. Efficient dye-sensitized solar cells with an organic photosensitizer featuring orderly conjugated ethylenedioxythiophene and dithienosilole blocks. *Chem Mater* 2010;22:1915–25; (b) Hagberg DP, Yum J-H, Lee H, De Angelis F, Marinado T, Karlsson KM. Molecular engineering of organic sensitizers for dye-sensitized solar cell applications. *J Am Chem Soc* 2008;130:6259–66; (c) Zhang G, Bala H, Cheng Y, Shi D, Lv X, Yu Q, et al. High efficiency and stable dye-sensitized solar cells with an organic chromophore featuring a binary  $\pi$ -conjugated spacer. *Chem Commun* 2009;16:2198–200; (d) Ko S-B, Cho A-N, Kim M-J, Lee C-R, Park N-G. Alkylxy substituted organic dyes for high voltage dye-sensitized solar cell: effect of alkylxy chain length on open-circuit voltage. *Dye Pigment* 2012;94:88–98.
- [4] Ito S, Miura H, Uchida S, Takata M, Sumioka K, Liska P. High-conversion efficiency organic dye-sensitized solar cells with a novel indoline dye. *Chem Commun* 2008;41:5194–6.
- [5] Chen Z, Li F, Huang C. Organic D- $\pi$ -A dyes for dye-sensitized solar cell. *Curr Org Chem* 2007;11:1241–58.
- [6] Wang Z-S, Cui Y, Dan-oh Y, Kasada C, Shinpo A, Hara K. Thiophene-functionalized coumarin dye for efficient dye-sensitized solar cells: electron lifetime improved by coadsorption of deoxycholic acid. *J Phys Chem C* 2007;111(19):7224–30.
- [7] Li C, Yum J-H, Moon S-J, Herrmann A, Eickemeyer F, Pschirer NG, et al. An improved perylene sensitizer for solar cell applications. *Chemosuschem* 2008;1(7):615–8.
- [8] (a) Yella A, Lee H-W, Tsao HN, Yi C, Chandiran AK, Nazeeruddin MK, et al. Porphyrin-sensitized solar cells with cobalt (II/III)-Based redox electrolyte exceed 12 percent efficiency. *Science* 2011;334:629–34; (b) Martínez-Díaz MV, de la Torre G, Torres T. Lighting porphyrins and phthalocyanines for molecular photovoltaics. *Chem Commun* 2010;46:7090–108; (c) Walter MG, Rudine AB, Wamser CC. Porphyrins and phthalocyanines in solar photovoltaic cells. *J Porphyrins Phthalocyanines* 2010;14:759–92; (d) Bessho T, Zakeeruddin SM, Yeh C-Y, Diau EW-G, Grätzel M. Highly efficient mesoscopic dye-sensitized solar cells based on donor–acceptor-substituted porphyrins. *Angewandte Chem Int Ed* 2010;49:6646–9.
- [9] Mori S, Nagata M, Nakahata Y, Yasuta K, Goto R, Kimura M, et al. Enhancement of incident photon-to-current conversion efficiency for phthalocyanine-sensitized solar cells by 3D molecular structuralization. *J Am Chem Soc* 2010;132:4054–5.
- [10] (a) Tian H, Yang X, Chen R, Pan Y, Li L, Hagfeldt A, et al. Phenothiazine derivatives for efficient organic dye-sensitized solar cells. *Chem Commun* 2007;3741–3; (b) Kim SH, Sakong C, Chang JB, Kim B, Ko MJ, Kim DH, et al. The effect of N-substitution and ethylthio substitution on the performance of phenothiazine donors in dye-sensitized solar cells. *Dye Pigment* 2013;97:262–71; (c) Kim SH, Kim HW, Sakong C, Namgoong JW, Park SW, Ko MJ, et al. Effect of five-membered heteroaromatic linkers to the performance of phenothiazine-based dye-sensitized solar cells. *Org Lett* 2011;13:5784–7.
- [11] (a) Eu S, Hayashi S, Umeyama T, Oguro A, Kawasaki M, Kadota N, et al. Effects of 5-membered heteroaromatic spacers on structures of porphyrin films and photovoltaic properties of porphyrin-sensitized  $TiO_2$  cells. *J Phys Chem C* 2007;111:3528–37; (b) Lin JT, Chen P, Yen Y, Hsu Y, Chou H, Yeh MP. Organic dyes containing furan moiety for high-performance dye-sensitized solar cells. *Org Lett* 2009;11:97–100.
- [12] (a) Li G, Zhou YF, Cao XB, Bao P, Jiang KJ, Lin Y, et al. Novel TPD-based organic D- $\pi$ -A dyes for dye-sensitized solar cells. *Chem Commun* 2009;16:2201–3; (b) Wu Y, Zhang X, Li W, Wang Z, Tian H, Zhu W. Hexylthiophene-featured D-A- $\pi$ -A structural indoline chromophores for coadsorbent-free and panchromatic dye-sensitized solar cells. *Adv Energy Mater* 2012;2:149–56.
- [13] (a) Tian H, Yang X, Cong J, Chen R, Liu J, Hao Y, et al. Tuning of phenoxazine chromophores for efficient organic dye-sensitized solar cells. *Chem Commun* 2009;41:6288–90; (b) Tian H, Yang X, Chen R, Hagfeldt A, Sun L. A metal-free “black dye” for panchromatic dye-sensitized solar cells. *Energy Environ Sci* 2009;2:674–7.
- [14] Karlsson KM, Jiang X, Eriksson KS, Gabrielsson E, Rensmo H, Hagfeldt A, et al. Phenoxazine dyes for dye-sensitized solar cells: relationship between molecular structure and electron lifetime. *Chem A Eur J* 2011;17:6415–24.
- [15] (a) Hara K, Wang Z-S, Sato T, Furube A, Katoh R, Sugihara H, et al. Oligothiophene-containing coumarin dyes for efficient dye-sensitized solar cells. *J Phys Chem B* 2005;109:15476–82; (b) Mikroyannidis JA, Kabanakis A, Balraju P, Sharma GD. Novel broadly absorbing sensitizers with cyanovinylene 4-nitrophenyl segments and various anchoring groups: synthesis and application for high-efficiency dye-sensitized solar cells. *J Phys Chem C* 2010;114:12355–63.
- [16] (a) Lin L-Y, Tsai C-H, Wong K-T, Huang T-w, Hsieh L, Liu S-h, et al. Organic dyes containing coplanar diphenyl-substituted dithienosilole core for efficient dye-sensitized solar cells. *J Org Chem* 2010;75:4778–85; (b) Chen R, Yang X, Tian H, Sun L. Tetrahydroquinoline dyes with different spacers for organic dye-sensitized solar cells. *J Photochem Photobiol* 2007;189:295–300.
- [17] Hagfeldt A, Grätzel M. Light-induced redox reactions in nanocrystalline systems. *Chem Rev* 1995;95(1):49–68.
- [18] Sakong C, Kim SH, Yuk SB, Namgoong JW, Park SW, Ko MJ, et al. Influence of solvent and bridge structure in alkylthio-substituted triphenylamine dyes on the photovoltaic properties of dye-sensitized solar cells 2012;7:1817–26.
- [19] Sakong C, Kim HJ, Kim SH, Namgoong JW, Park JH, Ryu J, et al. Synthesis and applications of new triphenylamine dyes with donor–donor–(bridge)–acceptor structure for organic dye-sensitized solar cells. *New J Chem* 2012;36:2025–32.
- [20] (a) Wang Q, Moser J-E, Grätzel M. Electrochemical impedance spectroscopic analysis of dye-sensitized solar cells. *J Phys Chem B* 2005;109:14945–53; (b) Bisquert J. Chemical capacitance of nanostructured semiconductors: its

- origin and significance for nanocomposite solar cells. *Phys Chem Chem Phys* 2003;5:5360–4.
- [21] (a) Kern R, Sastrawan R, Ferber L, Stangl R, Luther J. Modeling and interpretation of electrical impedance spectra of dye solar cells operated under open-circuit conditions. *Electrochim Acta* 2002;47:4213–25;  
(b) Kuang D, Ito S, Wenger B, Klein C, Moser JE, Humpry-Baker R, et al. High molar extinction coefficient heteroleptic ruthenium complexes for thin film dye-sensitized solar cells. *J Am Chem Soc* 2006;128:4146–54.
- [22] Kuang D, Uchida S, Humpry-Baker R, Zakeeruddin SM, Grätzel M. Organic dye-sensitized ionic liquid based solar cells: remarkable enhancement in performance through molecular design of indoline sensitizers. *Angewante Chem Int Ed* 2008;47:1923–7.